Macromolecules

ARTICLE

pubs.acs.org/Macromolecules

Stem Tilt in α-Form Single Crystals of Isotactic Polypropylene: A Manifestation of Conformational Constraints Set by Stereochemistry and Minimized Fold Encumbrance

Yan Cao,[†,‡] Ryan M. Van Horn,[†] Hao-Jan Sun,[†] Guoliang Zhang,[†] Chien-Lung Wang,[†] Kwang-Un Jeong,[§] Finizia Auriemma,[∥] Claudio De Rosa,[∥] Bernard Lotz,[*,⊥] and Stephen Z. D. Cheng[*,†]

[†]Department of Polymer Science, College of Polymer Science and Polymer Engineering, The University of Akron, Akron, Ohio 44325-3909, United States

[‡]Department of Materials Science and Engineering, South China University of Technology, Guangzhou 510640, China

[§]Polymer Bin Fusion Research Center, Department of Polymer Nano-Science and Technology, Chonbuk National University, Jeonju, Jeonbuk 561-756, Korea

[∥]Dipartimento di Chimia "Paolo Corradini", Università di Napoli "Federico II", Complesso Monte S. Angelo, Via Cintia, I-80126 Napoli, Italy

[⊥]Institut Charles Sadron (CNRS-Université de Strasbourg), 23, Rue du Loess, F-67034 Strasbourg, France

ABSTRACT: Two high molecular weight (MW) isotactic polypropylene (i-PP) samples, one containing a small amount of *rr* stereodefects denoted R1 and one conventional, commercial i-PP denoted S1, were used to grow single crystals in thin films at high temperatures (T_x = 145 °C for R1, T_x = 155 °C for S1). Elongated α_2-form lathlike single crystals could be found in these two samples, indicating that the growth of this type of single crystal is a general phenomenon in i-PP and is independent of the small amount of tacticity defects. On the basis of our selected area electron diffraction (SAED) experimental results, the stems in these lathlike single crystals were tilted at an unusual 17° angle around the *b*-axis (i.e., a rotation of 17° of the *c*-axis within the *ac*-plane toward the *a*-axis direction), while in the traditional scheme of the α-form in i-PP, the stem axis is understood to be normal to the fold surface. This 17° stem tilt in the α_2-form, lathlike single crystals grown at high T_x values appears to depend upon two constraints: (a) the conformational restrictions on chirality and clinicity of isotactic polyolefin stems linked by a fold, as analyzed by Petraccone et al. [Polymer 1986, 27, 1665; Eur. Polym. J. 1989, 25, 43], and (b) a minimized encumbrance at the fold surface can be achieved by those folds which start from and end on the chemical bonds normal to the fold surface with a favorable *gauche* conformation of i-PP chains. This is because in i-PP (and most isotactic polyolefins) with a helical stem conformation every other chemical bond is nearly parallel (in a *trans* conformation) or perpendicular (in a *gauche* conformation) to the stem axis (and thus, nearly within or normal to the fold surface). The combination of these two constraints favors a $(10\bar{2})$ fold surface in the i-PP case, as is observed in this study.

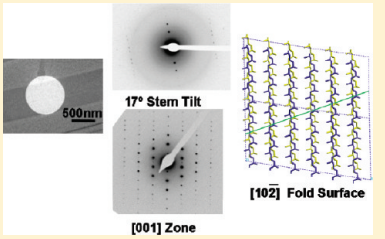

INTRODUCTION

A full understanding of the structural aspects of polymer lamellar crystals requires knowledge of both the crystal structure and the rules that govern the organization in chain folds. Elucidation of a polymer crystal, such as isotactic polypropylene, rests on well-established diffraction techniques (X-ray fiber analysis and electron diffraction for crystal polymorphs that cannot be oriented by mechanical means).[1−18] Analysis of the more elusive fold structure is more complex. The fold surface is a very thin, poorly organized layer, for which only a limited number of "local" techniques are available, among which are spectroscopic techniques (e.g., infrared or Raman). Decoration techniques in transmission electron microscopy (TEM) have been helpful: the polyethylene (PE) decoration technique that rests on the vaporization and condensation/crystallization of short PE rods makes it possible to determine the orientation of the outermost folds at a very local scale. The orientation of elongated stacks of rods helps visualize, e.g., the growth sectors in PE single crystals, isotactic polypropylene (i-PP) laths, and several other polymers.[19]

A different and fruitful means to gain insight into the fold structure (or, more precisely, a *representative* fold structure) takes into account the continuity of the chain when it leaves the crystal and enters the fold. This continuity may imply that certain features of the crystal structure have an impact or even impose constraints on the fold constitution and/or conformation. Reneker and Geil used this approach to explain the tilt of fold surfaces in PE single crystals.[20] Petraccone et al.[21,22] and Sadler et al.[23] applied this reasoning to isotactic polyolefins (i-PP and isotactic polystyrene, respectively). As developed later on in this publication, we will rely on the work of Petraccone et al.[21,22]

Received: December 19, 2010
Revised: April 4, 2011
Published: April 22, 2011

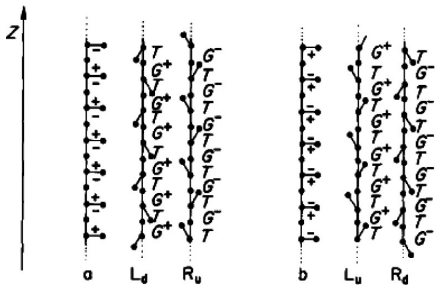

Figure 1. An i-PP polymer chain can be defined configurationally as the succession of (+) and (−) bonds along the backbone. Four types of helices with equivalent minimum conformational energy were sorted with **a** and **b** according to the different sequence of (+) and (−) bonds along the *z*-axis (chain axis). Reproduced with permission from ref 21. Copyright 1986 Elsevier.

Following their views, the succession of chemical bonds for a regular, isotactic polyolefin conformationally restricts the choice of stems that can be linked by a fold. These stems must be enantiomeric anticline and isochiral or enantiomeric antichiral and isocline. Note that pairs of chains with CH_3 side groups both oriented up or both oriented down are referred to as isoclined. Otherwise, they are anticlined. This requirement, in turn, must be compounded with the observed unit cell space groups.

In a further development along the same line, Lotz et al. considered that the most likely folds must be the least bulky ones.[24] When the main chain has a nearly crankshaft conformation, with some chemical bonds oriented parallel and others nearly normal to the fold surface, the latter ones are more likely to be the starting and ending points of the majority of folds. On these premises, the scrolling of (polyvinylidene fluoride) (PVDF) lamellae was explained by a difference in their fold constitution induced by the crystal structure.[25−27] Given the polar character of the γ-form of PVDF structure, folds with identical conformation have different volumes on opposite fold surfaces of the lamella. The folds are made of an odd number of carbons, and they differ by the presence of an extra CH_2 or an extra CF_2. The difference in volume (10 $Å^3$ per fold) induces different surface stresses and results in the observed spectacular scrolling of the γ-form of PVDF lamellae.

On the basis of the wealth of experimental results and detailed insights gained in earlier works by many groups on i-PP crystals in the past half-century, we are able to carry out the present investigation that deals with possible or likely fold conformations in crystals of i-PP in its most common α-form crystalline phase. The α-form of i-PP is based on a monoclinic unit cell with a = 0.665 nm, b = 2.096 nm, c = 0.65 nm and β = 99.80° that was established by Natta and Corradini more than a half-century ago.[28] Later on, both disordered and ordered crystals regarding to the "up" or "down" CH_3 orientation in the α-form unit cell were observed in the wide-angle X-ray diffraction and differential scanning calorimetry (DSC) analysis.[29−37] Following Hikosaka and Seto,[35] the metastable crystalline form having random "up" or "down" CH_3 orientations with the space group $C2/c$ is named the α_1-form, and the more stable form having ordered CH_3 orientations is named the α_2-form with the space group of $P2_1/c$. Viewing along the *b*-axis of the α-form unit cell, "up" or "down" CH_3 orientation determined by CH_3 tetrahedral geometry alternates every two antichiral layers in the α_2-form unit cell, while random CH_3 orientation exists in the α_1-form unit cell. Four types of helices with equal conformational free energy (Figure 1) can be constructed: a left-hand helix with "up" CH_3 (L_u), a left-hand helix with "down" CH_3 (L_d), a right-hand helix with "up" CH_3 (R_u), and a right-hand helix with "down" CH_3 (R_d).[21,22] Experimentally, the α_2-form displays both odd and even $h + k$ reflections, whereas for the α_1-form only $h + k$ = even reflections are observed.[29−37] Furthermore, the more ordered α_2-form only can grow at low supercooling, and the less ordered α_1-form forms at high supercooling.[38,39]

Following Corradini et al.,[40] as illustrated in Figure 1, a defect-free i-PP chain can be defined configurationally as a succession of (+) and (−) bonds along the backbone axis. The (+) and (−) bonds are defined as two adjacent bonds connecting to the same carbon atom with two different substituents, CH_3 and H, along the backbone axis. The (+) and (−) bonds are counted respectively as a clockwise or counterclockwise rotation from the substituents CH_3 to H viewing along one C−C bond's projection. Furthermore, the 3-fold helical conformation in i-PP is generated by the alternation of a *trans* and a *gauche* bond along the chain axis to construct either right- or left-handed helices. It is worth noting that the (+) bonds tend to assume only G^+ or T conformations, while the (−) bonds tend to assume only G^- or T conformations. Moreover, the lateral CH_3 substituent groups as tetrahedral connections are either pointing "up" or pointing "down" with respect to a vertical backbone axis. As shown in Figure 1, four helices, L_u, L_d, R_u, and R_d have equal minimum conformational free energy.

The α-form of i-PP is original among polyolefins in that it is based on 3-fold helices that pack in an unusual monoclinic unit cell, whereas most polyolefins pack in tetragonal or trigonal cells. For the latter (tetragonal or trigonal) cell symmetries, the chains are normal to the lamellar surface. Surprisingly, this normal alignment usually holds true for i-PP, in spite of its monoclinic cell geometry, but the fold surface becomes the $(10\bar{6})$ plane.

In fact, earlier observations indicated that the stems of i-PP single crystals in α-form are tilted away from the lamellar surface normal. A 10° stem tilt would be expected based on the α-form monoclinic unit cell geometry (β = 99.8°) if the fold surface were the (001) plane and parallel to the *a*-axis (the long axis) of the single crystal substrate. Conspicuous stem tilts can be inferred from α−α lamellar branching angles that sometimes differ significantly from the normally expected 80° (or 100°) when the stems are oriented normal to the fold surface.[41−45] Recently, we have reported that the stems in the α-form crystal, from which the γ-form single crystal epitaxial overgrowth crystallized in i-PP thin films, may be tilted at a significant angle (up to about 25°) to the fold surface normal of the α-form.[46] No explanation of this behavior could be given at that time. We have therefore reexamined this issue by using both a specifically synthesized sample and a commercial sample. It is observed that in both samples when crystallization takes place at high crystallization temperatures (T_x), the stems in the single crystal are consistently tilted at a (more accurate) 17° angle to the fold surface around the *b*-axis of the i-PP α-form unit cell. This leads to a fold surface parallel to the $(10\bar{2})$ plane.

This fold surface appears quite logical if one assumes that the folds must leave and re-enter the crystal with chemical bonds in a *gauche* conformation which is nearly normal to the fold surface (and thus, reducing the overall volume of the fold), while the *trans* conformation is much less probable since it is nearly parallel to the fold surface. Furthermore, the folds do indeed follow the selection rules on chirality and clinicity indicated by Petraccone et al. Both criteria appear to be of general applicability (the last one at least for polyolefins) and help establish guiding principles in the "crystallographic" analysis of polymer crystal folds.

EXPERIMENTAL SECTION

Materials and Sample Preparation. A stereodefective i-PP fraction prepared with a highly regiospecific metallocene catalyst (R1), as described in refs 47 and 48, and a normal commercial i-PP (Sigma-Aldrich) sample (S1) were used in this study. The major microstructure characteristics (molecular weight, M_w, and polydispersity) and melting temperatures are listed in Table 1. The molar mass and molar mass distributions of i-PP were determined by gel permeation chromatography (GPC) at 135 °C with a Waters instrument GPCV 2000 equipped with refractive index and viscometer detectors, using a set consisting of four PS columns: 105, 104, 103, and 102 Å (pore size) with 10 μm particle size. The carrier solvent was *o*-dichlorobenzene with a flow rate of 1.0 mL min^{-1}. The calibration curve was established with polystyrene standards. Solution ^{13}C NMR spectra have been recorded with a 300 MHz Brüker Advance spectrometer at 100 °C on dilute solution in 1,1,2,2-tetrachloroethane-d_2. Assignment of the resonances to the different stereosequences (pentads) has been performed according to the description by Busico et al.[49] The sample R1 crystallizes at T_x = 145 °C in 21 days, and the sample S1 crystallizes at 155 °C in 12 h. Both samples form the α-form crystals.

Thin films were prepared for TEM and atomic force microscopy (AFM) experiments by casting i-PP/octane solution with a concentration of 0.005% (w/v) at 110 °C for R1 and 120 °C for S1 onto carbon-coated mica surfaces. The concentration was low enough so that the films (about 16 nm thick) did not entirely cover the mica surface. The samples were first heatedto 180 °C to evaporate the solvent. They were then melted at 180 °C for 5 min in a hot stage (Mettler FP90) and quickly transferred to another hot stage (a second Mettler FP90) preset at the isothermal crystallization temperature (T_x: 145 or 155 °C) and left to crystallize in a dry nitrogen atmosphere. AFM experiments were performed on the crystallized samples straight from the thermal treatment without further preparation. For TEM observations, sometimes the thin films were shadowed with platinum and decorated by PE rods.

Table 1. Molecular Characteristics of the i-PP R1 and S1

samples	mol wt (M_w)	T_m (°C)	[mmmm] (%)	[rr] (%)	polydispersity
R1	110 000	144[a]	89.0	2.3[b]	2
S1	200 000	160−165	90.0	3.0[b]	3.1

[a] The reason that T_x = 145 °C in our experiments is higher than the T_m = 144 °C is that the T_m = 144 °C was observed by DSC when R1 was crystallized at a lower temperature. This melting temperature does not represent the equilibrium melting temperature (T_m^0) of this i-PP, but is much lower than T_m^0. [b] R1 was polymerized using the homogeneous metallocene catalyst,[46] and S1 was polymerized using the heterogeneous Ziegler−Natta catalyst. The 3% here only represents an average value of the [rr] but does not illustrate the distribution of the steric defects.[47]

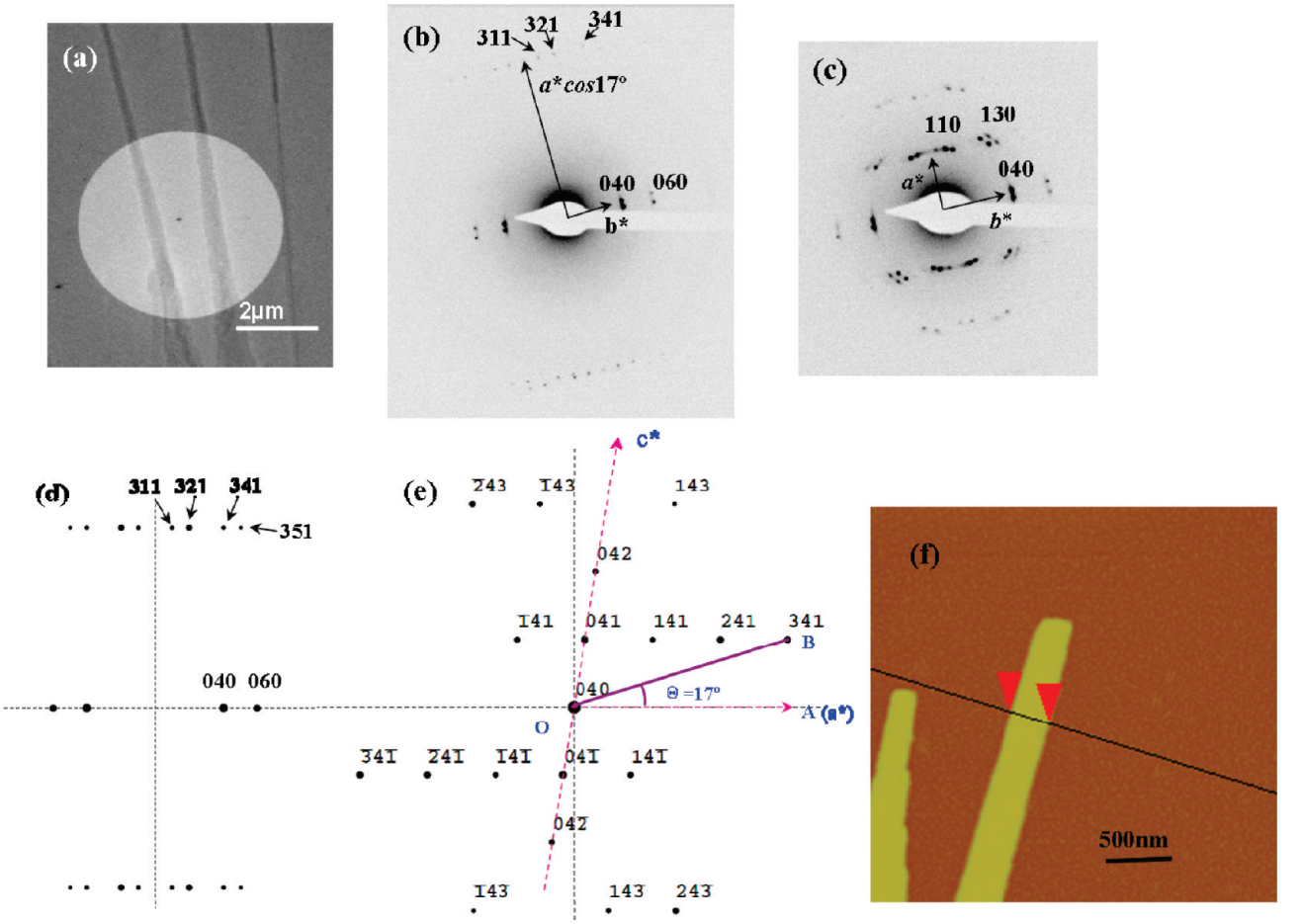

Figure 2. (a) BF image of three i-PP α_2-phase single crystals isothermally crystallized from the thin-film melt at T_x = 145 °C for 21 days. (b) SAED pattern exhibits 311, 321, and 341 diffraction spots of two α_2-phase single crystals in (a). (c) SAED of the 17° tilt away from the thin film normal around the b^*-axis within the *ac*-plane. (d) A calculated ED pattern of the α_2-phase with the $[10\bar{3}]$ zone utilizing Cerius^2 crystallographic package. (e) A calculated ED pattern of the α_2-phase single crystal at the fourth layer with the [010] zone utilizing Cerius^2 crystallographic package. (f) AFM image of i-PP α-phase crystal morphology (T_x = 145 °C for 21 days). The morphology was observed at room temperature.

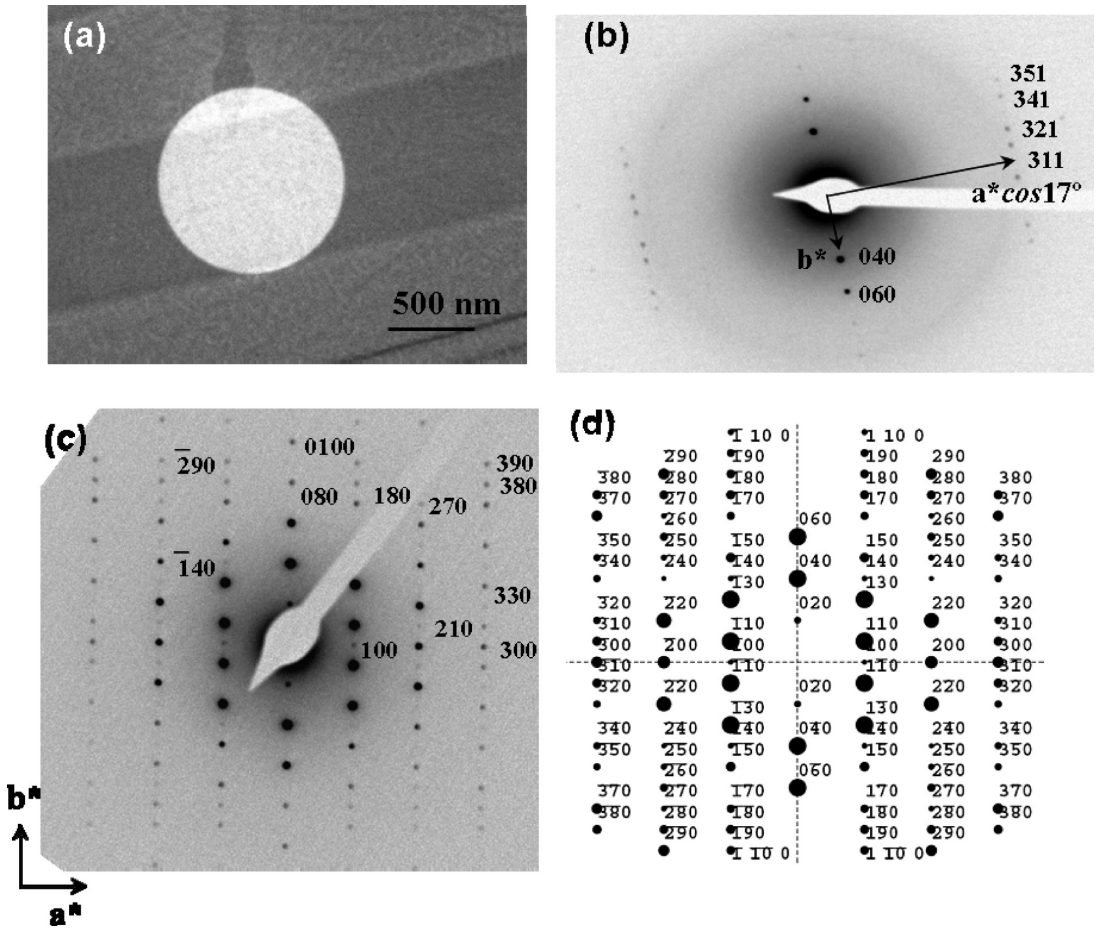

Figure 3. (a) TEM bright field morphology of the α_2-phase single crystal grown from thin film melt at 155 °C by using the commercial sample S1. (b) SAED pattern of the $[10\bar{3}]$ zone of the α_2-phase single crystal (circled area in Figure 2a) using sample S1. (c) Selected-area 17°-tilt ED pattern of the [001] zone of the α_2-phase single crystal. (d) A calculated ED pattern of the α_2-phase with the [001] zone utilizing the atomic coordinates of Immirzi and Iannelli.

The sample and carbon film were then floated on distilled water and picked up on copper grids.

Equipment and Experiments. The overall crystal morphology was observed under phase contrast optical microscopy (Olympus, BH-2) and in bright field (BF) TEM (Philips Tecnai-12) at an accelerating voltage of 120 kV. Selected area electron diffraction (SAED) experiments were carried out using a ± 60° tilting stage to obtain SAED patterns at different zone axes. In order to extend the lifetime of the crystals under the electron beam, the grids were scanned at very low beam intensity by defocusing the diffraction pattern. The *d*-spacings were calibrated using a TlCl standard. Molecular modeling and analysis of the diffraction patterns were performed using the Accelrys Cerius[2] package.

AFM (Digital Instruments, now Veeco Nanoscope IIIA) was used to examine the single crystals while still on the mica support. A 100 μm scanner was selected. Both height and phase images were recorded in the tapping mode. The scan rate was 1−3 Hz when acquiring low-magnification images (resolution: 512 × 512 pixels).

RESULTS

17° Tilt of the Stems in the α_2-Form Single Crystal of i-PP Grown in the Thin Film Melt. Figure 2a is a TEM BF image of three elongated lathlike α-form single crystals isothermally crystallized in the stereodefective i-PP sample R1 at T_x = 145 °C for 21 days. Unlike the crystal grown at 120 °C where the γ-form crystals are epitaxially overgrown on both sides of the single crystal,[46] Figure 2a does not show any of the γ-form overgrowth. Figure 2b is a SAED pattern of two of the three crystals shown in Figure 2a (the circled area shown in Figure 2a) with two slightly misoriented sets of diffraction spots. One line of strong diffraction spots is along the b^*-axis, and the weak lines of diffraction spots are the third layers above and below, but parallel to the b^*-axis. No full set of $hk0$ diffractions can be observed, indicating that the stems of i-PP are not normal to the substrate (also, the single crystal fold surface). Thus, it is not a $[00l]$ zone ED pattern. The logical deduction is that the stems are tilted at an angle, θ, away from the normal to the single crystal fold surface.

After the single crystal was rotated clockwise or counterclockwise 17° along the b^*-axis (in this case, the b^*-axis is parallel to the b-axis) depending on the a^*-axis orientation of the single crystals under TEM (see below), a full $hk0$ diffraction $[00l]$ zone pattern can be observed as shown in Figure 2c. Therefore, the c-axis of the α-form single crystal is tilted 17° away from the surface normal within the ac-plane toward the a-axis. As a result, we can determine that the SAED pattern shown in Figure 2b corresponds to the $[10\bar{3}]$ zone axis. According to the d-spacing calculation, the diffraction spots in Figure 2b are indexed as 040, 060, 311, 321, and 341. The hkl diffraction spots possess both odd and even values of $h + k$, indicating that the more ordered

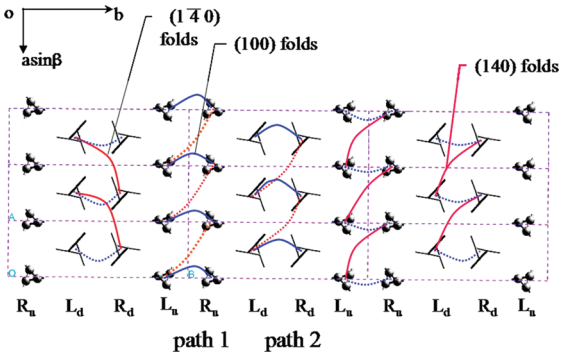

Figure 4. Top view of the $a(\sin\beta)b$-plane projection of the α-form unit cell of i-PP with the space group $P2_1/c$. Two different fold pathways are respectively designated with the stick−ball model and cylinder model. Pathway 1 has the (100) folds with "up" CH_3 orientation and the (140) folds with "down" CH_3 orientation. Pathway 2 has the (100) folds with "down" CH_3 orientation and the (140) folds with "up" CH_3 orientation.

α_2-form single crystal with a $P2_1/c$ space group has been produced, rather than the less ordered α_1-form single crystals with the $C2/c$ space group (in the α_1-form, only $hk1$ spots with $h + k$ even are observed). Furthermore, it should be noted that the stem tilt can only be toward the a-axis, but not toward the negative a-axis because the reflections seen are $3k1$ and not $\bar{3}k1$.

Since Figure 2b is the ED pattern of the α_2-form single crystal, we used the current Cerius^2 crystallographic package and input the atomic fractional coordinates given by Hikosaka and Seto,[35] Mencik,[36] and Immirzi and Iannelli[37] to simulate the ED pattern. The calculated pattern of the $[10\bar{3}]$ zone of the α_2-form single crystal based on the refined model of Immirzi and Iannelli[37] is shown in Figure 2d. Indeed, these simulation results are consistent with the SAED pattern in Figure 2b and confirm that the single crystal is the α_2-form. Because the stem orientation (the c-axis) in the single crystal was rotated 17° around the b-axis, the series of $3k1$ diffraction spots intersect with the Ewald's sphere and appear in the diffraction pattern of Figure 2b as shown in Figure 2e. The [010] zone of the α_2-form single crystal indicates that the 17° rotation of the crystal around the b-axis in the ED experiments is consistent with the θ angle in the reciprocal lattice in Figure 2e. The $[10\bar{3}]$ zone axis and the corresponding 17° stem tilt indicate that the lamellar fold surface is the $(10\bar{2})$ plane (the $[10\bar{3}]$ zone axis is 0.3° away from the $(10\bar{2})$ plane normal). The observation of this $(10\bar{2})$ fold surface will be an essential ingredient of the discussion to follow. Finally, Figure 2f shows an AFM image of an i-PP (R1) lathlike α_2-form single crystal crystallized at T_x = 145 °C for 21 days. The crystal lamellar thickness and width are 24 and 380 nm, respectively.

The stem tilt in the α-form of i-PP single crystals observed here is very reminiscent of a similar one reported by Lovinger and Keith for the α-form single crystals of PVDF.[50] In PVDF, the single crystals are elongated along the b-axis. The stems are also tilted by 25° with respect to the b-axis with a fold surface being close to the (102) plane.

Up to now, all the experimental results and analyses are based on the α_2-form single crystals of the specially synthesized sample R1 that contains a small amount of stereodefects. The next objective was to check if this observation is linked to a specific molecular feature such as in the sample R1 or if it applies to the α_2-form of i-PP in general. It is known that differences in chemical structure for i-PP may dramatically impact the crystal structure and morphology, such as the development of the γ-phase. We then chose a commercial sample, S1. Since its melting point is about 15−20 °C higher than that of R1, the crystallization of S1 was carried out at 155 °C rather than 145 °C. Even at such a high T_x, the crystallization kinetics were still faster for S1 compared to R1.[51,52]

Figure 3a is a TEM BF image of a section of a ribbonlike lamellar α-form single crystal of the commercial sample S1. Figure 3b is its SAED pattern that is identical to the one shown in Figure 2b. According to the simulation shown in Figure 2d, the diffraction spots in this pattern can be identified as the 040 and 060 on the zero layer and the 311, 321, 341, and 351 on the other lines. These diffraction spots indicate again a 17° tilt of the stems in the α_2-form single crystal. Therefore, the 17° tilt of the stems is a general feature of i-PP lamellae in the more "perfect" α_2-form single crystals, at least when crystallized in the higher end of the crystallization range.

A SAED pattern after 17° rotation of the crystal around the b-axis shows the [001] zone pattern of the α_2-form (Figure 3c). A simulation pattern calculated with the Cerius^2 package is shown in Figure 3d. Comparing Figure 3d with Figure 3c, the calculated pattern displays the major features of the experimentally observed SAED pattern. However, some slight adjustments of the structure may be needed in order to generate, e.g., the 080, 0100, 210, 330, and 390 diffraction spots that appear in the experimental SAED pattern. Spots with $h + k$ = odd, for example, the 100, $\bar{1}40$, 180, 210, 270, $\bar{2}90$, 300, and 380 diffraction provide again clear evidence that the single crystal belongs to the α_2-form of i-PP.

DISCUSSION

Conformational Constraints in the Folds of α_2-Form in i-PP Crystals. Why is the stem tilt specifically 17° rather than any other angles in α_2 form single crystals of i-PP? Here, we attempt to analyze how chain folding takes place under *conformational constraints* while taking into account the *fold encumbrance* for different fold surfaces.

For the four kinds of helices, L_u, L_d, R_u, and R_d, as illustrated in Figure 1, with equal minimum free energy, there are C_4^2 possible ways (6 ways) to connect two different neighboring stems: the (R_u, R_d), (R_u, L_d), (R_u, L_u), (L_u, L_d), (L_u, R_d), and (L_d, R_d). Following Petraccone et al.[21,22] in the α_2-form single crystal of i-PP, a fold can only bridge two enantiomeric helical stems, and there must be a reversal in the axis direction of the (+) and (−) bonds. Thus, a fold can only connect two different helical stems under one of two following conditions: either antichiral and isocline or isochiral and anticline. The folds between stems in the single crystal cannot take place for (R_u, L_d) and (L_u, R_d); folds are only possible for (R_u, R_d), (R_u, L_u), (L_u, L_d), and (L_d, R_d).

Figure 4 is the top view of the $a(\sin\beta)b$-plane projection of the unit cell. Two sets of enantiomeric helical stems are represented by either the ball−stick or cylinder model. In the premise of adjacent-reentry folds, folds are not allowed between two isochiral and anticline (R_u, R_d) or (L_u, L_d) stems. Consequently, the folds can only connect two antichiral and isocline (L_u, R_u) or (L_d, R_d) stems. This constraint may be released only by allowing the formation of nonadjacent re-entry folds (or, of course, structural disorder and lower cell symmetry such as in the α_1-form).

Figure 4 also shows that the folds can only be allowed within the two antichiral and isocline layers. This principle results in three kinds of folds: the (140) or $(1\bar{4}0)$, and (100) folds. Since the stems involved in the (140) folds and the $(1\bar{4}0)$ folds in the

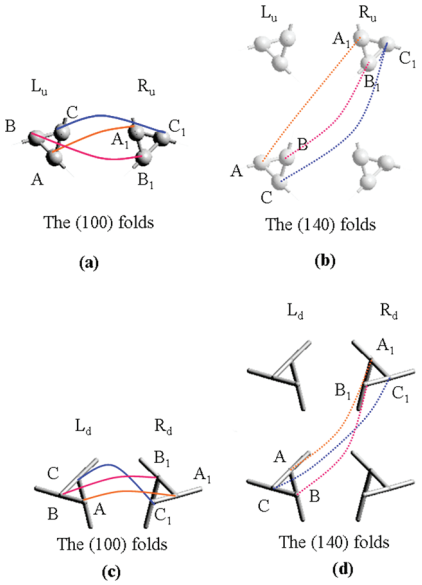

Figure 5. Three possible fold trajectories AA_1 (yellow), BB_1 (magenta), and CC_1 (blue) composed of a fold for every pair of antichiral and isocline stems respectively for (a) the (100) folds with "up" CH_3 orientation, (b) the (140) folds with "down" CH_3 orientation, (c) the (100) folds with "down" CH_3 orientation, and (d) the (140) folds with "up" CH_3 orientation.

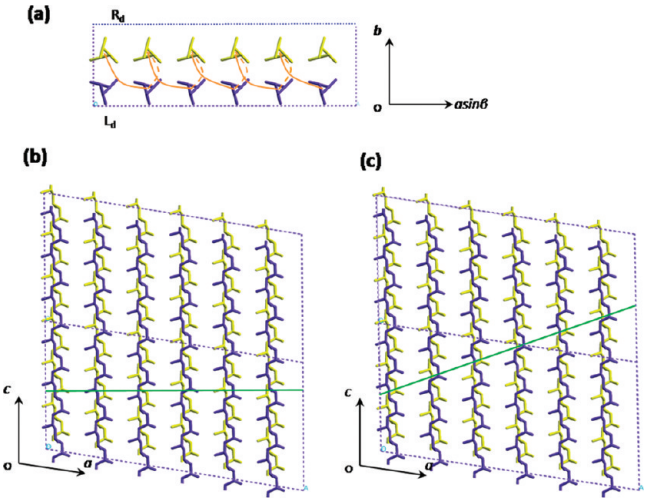

Figure 6. (a) One fold path (R_d, L_d) made up by alternating the (140) folds and the (100) folds in the $a(\sin\beta)b$-plane projection. (b) The $(10\bar{6})$ fold surface denoted a green line in the *ac*-plane projection. (c) The $(10\bar{2})$ fold surface denoted a green line in the *ac*-plane projection.

α_2-form unit cell are symmetrically and geometrically identical, only the (140) fold will be discussed in detail. If a (140) fold forms on the top or bottom fold-surface of a single crystal, the next fold that forms on the opposite (the bottom or top) fold-surface of the single crystal must be a (100) fold. Therefore, the fold pathways should be alternating between the (100) and (140) folds on both sides of the fold surfaces. In detail, the (L_u, R_u) pathway has two possible folds: the short (100) folds with "up" CH_3 orientation (Figure 5a) and the long (140) folds with "down" CH_3 orientation (Figure 5b). The (L_d, R_d) pathway similarly has the short (100) folds with "down" CH_3 orientation (Figure 5c) and the long (140) folds with "up" CH_3 orientation (Figure 5d). All of these folds could lead to two nonequivalent ("up" and "down") adjacent re-entry fold pathways (paths 1 and 2, respectively, in Figure 4) analyzed by Petraccone et al.[21,22] Furthermore, there are three possible fold trajectories of the AA_1 (yellow), BB_1 (magenta), and CC_1 (blue) as shown in Figure 5a−d.

Selection of Folds According to the Encumbrance in the Fold Surface. In the previous section, the folds following the requirements of conformational constraints have been analyzed. However, there are additional constraints applied to the folds by the overcrowding in the fold surface. In order to reduce the fold encumbrance, the folds with bonds oriented nearly normal to the fold surface when they leave and re-enter the crystal are more favorable. The i-PP polymer possesses a nearly crankshaft chain conformation, and the folds thus leave and re-enter the crystal only via local *gauche* conformations.

Figure 6a illustrates the (140) and (100) folds on the top and bottom of a α_2-form single crystal. Figure 6b,c shows two *ac*-projections of the i-PP stems in the crystal. The green lines in both figures represent the $(10\bar{6})$ and $(10\bar{2})$ planes, respectively. Looking at one fold path connecting (R_d, L_d) within the *ac*-plane as an example, as shown in both Figure 6b,c, the conformations leaving and entering the crystal (beginning and end of the fold, across the green lines) must be all in the *gauche* conformation (nearly normal to the fold surface) rather than the *trans* conformation (nearly parallel to the fold surface). At the $(10\bar{2})$ fold surface generated by the 17° stem tilt as shown in Figure 6c, the conformations across this fold surface are all *gauche*, which are nearly perpendicular to the crystal surface. On the other hand, the conformations across the $(10\bar{6})$ fold surface alternate between *gauche* and *trans* within the *ac*-plane, where no stem is tilted in the single crystal. Therefore, one can expect that folds generated in the $(10\bar{2})$ plane are thermodynamically more favorable. Furthermore, the $(10\bar{2})$ fold surface also provides a relatively easy organization (a lower free energy) for the folds leaving and entering on the (100) folds in the *gauche* conformations between the L_d and R_d (or the L_u and R_u), while this may not be the case for the $(10\bar{6})$ fold surface. Hence, the $(10\bar{2})$ fold surface with the 17° tilt of the stems is favored for the fold orientations along the (140) plane [or the $(1\bar{4}0)$ plane] and the (100) plane for the α_2-form i-PP single crystals grown at high T_x values under the premise that the folds are all adjacent re-entrant.

It should be noted that when the T_x values decreases, we have observed that some of the single crystals possess stems that are normal to the fold surface. When the T_x value is further decreased to the region where only the α_1- single crystals are formed, the stems of these α_1-form single crystals are perpendicular to the fold surface. This indicates that after the "up" and "down" CH_3 group orientation is lost in the α_1-form i-PP single crystal, the restraints of the adjacent re-entry folds of the α_2-form i-PP single crystals (as shown in Figure 4) are also more or less removed. In this case, the single crystals adopt the $(10\bar{6})$ fold surface. This conclusion has also been reached via molecular dynamics analyses based on solid-state NMR results reported by Miyoshi et al.[39]

Since there are three kinds of fold orientations: the (100) folds, the (140) folds, and the $(1\bar{4}0)$ folds on the fold surface of a single crystal and each of these folds has three possible trajectories (AA_1, BB_1, and CC_1 as shown in Figure 5), this may lead to an orientation disorder of the folds of the α_2-form single crystals at their folded surface. As a result, multiple orientations of the decorated PE rod crystals may be observed. This is what we

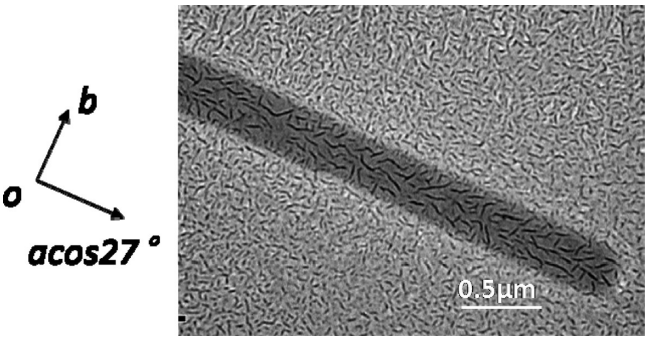

Figure 7. TEM BF image of the α_2-form single crystal isothermally crystallized from the thin film melt (R1) at T_x = 145 °C for 21 days after PE decoration and subsequent platinum shadowing.

observed as shown in Figure 7. While the (100) fold orientation manifested in the macroscopic (100) growth sectors of the solution grown i-PP single crystals observed utilizing the PE decoration method by Wittmann and Lotz,[19] a mixture of the (100) and the (140) or (1$\bar{4}$0) folds is expected in this case of the present study based on the PE decoration results.

CONCLUSION

In lamellar single crystals of i-PP in its α_2-form modification grown at high T_x values, the 17° tilt stem orientation away from the fold surface normal toward the *a*-axis within the *ac*-plane of the single crystals has been revealed via TEM SAED results for both specifically synthesized (R1) and industrial (S1) samples. The zone axis of the fold surface is thus the [10$\bar{3}$] zone, and the fold surface is the (10$\bar{2}$) plane. This 17° tilt of the stems in the α_2-form is a rather general feature apparently independent of the conformational stereodefects when the defect concentration is relatively low, and thus, they must be largely excluded from the i-PP single crystals. It is known that in isotactic polyolefins there is a conformational restriction on the kind of stems that are linked by folds. These two stems must be enantiomeric antichiral and isocline. Because the α_2-form single crystal has the space group $P2_1/c$, their "up" or "down" CH_3 orientation alternately changes along the *b*-axis in every antichiral bilayer; isochiral and anticline stems cannot be side-by-side and connected by adjacent re-entry folds. Therefore, the adjacent re-entry folds could only occur between two neighboring antichiral and isocline stems, such as (L_u, R_u) or (L_d, R_d). A fold linking two stems may have three possible orientations along the (100), (140), or (1$\bar{4}$0) crystallographic planes. For the (140), (1$\bar{4}$0), and (100) folds, the 17° tilt in the α_2-form single crystal indicates that the stems are in the *gauche* conformation when they start from (leave) and end on (re-enter) the single crystal surface at the (10$\bar{2}$) plane for the purpose of reducing the fold surface free energy. Furthermore, under the premise of adjacent re-entry folding, the (140) and (1$\bar{4}$0) folds must be coupled with the (100) folds on the opposite fold surface to appear as pairs. Since the fold surface may contain the (140), (1$\bar{4}$0), and (100) folds, the overall fold orientation on the surface could be disordered. The analysis carried out here provides a possible understanding of the chain folding behavior. The combination of steric (fold encumbrance) and conformational (specific association of stems) constraints promotes the 17° stem tilt in the α_2-form crystals in i-PP, especially in case of adjacent re-entry folding.

AUTHOR INFORMATION

Corresponding Author

*E-mail: bernard.lotz@ics-cnrs.unistra.fr (B.L.); scheng@uakron.edu (S.Z.D.C.).

ACKNOWLEDGMENT

This work was supported by the National Science Foundation (DMR-0906898) and a graduate fellowship provided by the Chevron-Phillips Chemical Co. The authors thank Dr. F. Khoury for helpful discussions and the Chinese Scholarship Council for financial support.

REFERENCES

(1) Keith, H. D.; Padden, F. J., Jr.; Walter, N. M.; Wickoff, H. W. *J. Appl. Phys.* **1959**, *30*, 485.
(2) Addink, E. J.; Beintema, J. *Polymer* **1961**, *2*, 185.
(3) Kardos, J. L.; Christiansen, A. W.; Baer, E. *J. Polym. Sci.* **1966**, *A-2* (4), 777.
(4) Padden, F. J., Jr.; Keith, H. D. *J. Appl. Phys.* **1959**, *30*, 1479.
(5) Padden, F. J., Jr.; Keith, H. D. *J. Appl. Phys.* **1966**, *37*, 4013.
(6) Padden, F. J., Jr.; Keith, H. D. *J. Appl. Phys.* **1973**, *44*, 1217.
(7) Lovinger, A. J.; Chua, J. O.; Gryte, C. C. *J. Polym. Sci., Polym. Phys. Ed.* **1977**, *15*, 641.
(8) Lotz, B.; Wittmann, J. C.; Lovinger, A. J. *Polymer* **1996**, *37*, 4979.
(9) Lotz, B.; Graff, S.; Wittmann, J. C. *J. Polym. Sci., Polym. Phys. Ed.* **1986**, *24*, 1541.
(10) Brückner, S.; Meille, S. V.; Petraccone, V.; Pirozzi, B. *Prog. Polym. Sci.* **1991**, *16*, 361.
(11) Lotz, B.; Kopp, S.; Dorset, D. *C. R. Acad. Sci. Paris* **1994**, *319* (Ser. IIb), 187.
(12) Lotz, B.; Graff, S.; Wittmann, J. C. *J. Polym. Sci.,Polym. Phys. Ed.* **1986**, *24*, 2017.
(13) Lotz, B.; Graff, S.; Straupé, C.; Wittmann, J. C. *Polymer* **1991**, *32*, 2902.
(14) Cheng, S. Z. D.; Janimak, J. J.; Zhang, A. Q.; Hsieh, E. T. *Polymer* **1991**, *32*, 648.
(15) Cheng, S. Z. D.; Janimak, J. J.; Zhang, A. Q.; Cheng, H. N. *Macromolecules* **1990**, *23*, 298.
(16) Janimak, J. J.; Cheng, S. Z. D.; Giusti, P. A. *Macromolecules* **1991**, *24*, 2253.
(17) Brückner, S.; Meille, S. V. *Nature* **1989**, *340*, 455.
(18) Meille, S. V.; Ferro, D. R.; Brückner, S.; Lovinger, A. J.; Padden, F. J., Jr. *Macromolecules* **1994**, *27*, 264.
(19) Wittmann, J. C.; Lotz, B. *J. Polym. Sci., Polym. Phys. Ed.* **1985**, *23*, 205.
(20) Geil, P. H. *Polymer Single Crystals*; John Wiley & Sons Inc.: New York, 1963.
(21) Petraccone, V.; Pirozzi, B.; Meille, S. V. *Polymer* **1986**, *27*, 1665.
(22) Petraccone, V.; Pirozzi, B.; Meille, S. V. *Eur. Polym. J.* **1989**, *25*, 43.
(23) Sadler, D. M.; Spells, S. J.; Keller, A.; Guenet, J. M. *Polym. Commun.* **1984**, *25*, 290.
(24) Lotz, B.; Thierry, A.; Schneider, S. *C. R. Acad. Sci. (Paris)* **1998**, *IIc*, 609.
(25) Lotz, B.; Cheng, S. Z. D. *Polymer* **2005**, *46*, 577.
(26) Padden, F. J., Jr.; Keith, H. D. *Macromolecules* **1996**, *29*, 7776.
(27) Vaughan, A. S. *J. Mater. Sci.* **1993**, *28*, 1805.
(28) Natta, G.; Corradini, P. *Nuovo Cimento Suppl.* **1960**, *15*, 40.
(29) Corradini, P.; Petraccone, V.; Pirozzi, B. *Eur. Polym. J.* **1983**, *19*, 299.
(30) Naiki, M.; Kikkawa, T.; Endo, Y.; Nozaki, K.; Yamamoto, T.; Hara, T. *Polymer* **2001**, *42*, 5471.
(31) Corradini, P.; Giunchi, G.; Petraccone, V.; Pirozzi, B.; Vidal, H. M. *Gazz. Chim. Ital.* **1980**, *110*, 413.

(32) De Rosa, C.; Guerra, G.; Napolitano, R.; Petraccone, V.; Pirozzi, B. *Eur. Polym. J.* **1984**, *10*, 937.
(33) Auriemma, F.; Ruiz de Ballesteros, O.; De Rosa, C.; Corradini, P. *Macromolecules* **2000**, *33*, 8764.
(34) De Rosa, C.; Guerra, G.; Napolitano, R.; Petraccone, V.; Pirozzi, B. *J. Therm. Anal.* **1985**, *30*, 1331.
(35) Hikosaka, M.; Seto, T. *Polym. J.* **1973**, *5*, 111.
(36) Mencik, Z. *J. Macromol. Sci., Phys.* **1972**, *6*, 101.
(37) Immirzi, A.; Iannelli, P. *Macromolecules* **1988**, *21*, 768.
(38) Cheng, S. Z. D. *Phase Transitions in Polymers:The Role of Metastable States*; Elsevier: Amsterdam, 2008.
(39) Miyoshi, T.; Mamun, A.; Hu, W. *J. Phys. Chem.* **2010**, *114*, 92.
(40) Corradini, P. In *The Stereochemistry of Macromolecules*; Ketley, A. D., Ed.; Marcel Dekker: New York, 1968; Vol. III, pp 1−60.
(41) Khoury, F. *J. Res. Natl. Bur. Stand.* **1966**, *70A*, 29.
(42) Lovinger, A. J. *J. Polym. Sci., Polym. Phys. Ed.* **1983**, *21*, 97.
(43) Binsbergen, F. L.; De Lange, B. G. M. *Polymer* **1968**, *9*, 23.
(44) Selikhova, V. I.; Zubov, Yu. A.; Markova, G. S.; Kargin, V. A. *Polym. Sci. U.S.S.R.* **1965**, *7*, 232.
(45) Clark, E. S.; Spruiell, J. E. *Polym. Eng. Sci.* **1976**, *16*, 176.
(46) Cao, Y.; Van Horn, R. M.; Tsai, C.-C.; Graham, M. J.; Jeong, K.-U.; Auriemma, F.; De Rosa, C.; Lotz, B.; Cheng, S. Z. D. *Macromolecules* **2009**, *42*, 4758.
(47) De Rosa, C.; Auriemma, F.; Circelli, T.; Waymouth, R. M. *Macromolecules* **2002**, *35*, 3622.
(48) Auriemma, F.; De Rosa, C. *Macromolecules* **2002**, *35*, 9057.
(49) Busico, V.; Cipullo, R.; Monaco, G.; Vacatello, M.; Segre, A. L. *Macromolecules* **1997**, *30*, 6251.
(50) Lovinger, A. J.; Keith, H. D. *Macromolecules* **1996**, *29*, 8541.
(51) Keller, A.; Cheng, S. Z. D. *Polymer* **1998**, *39*, 4461.
(52) Cheng, S. Z. D.; Keller, A. *Annu. Rev. Mater. Sci.* **1998**, *28*, 533.